

Rotating magnetic fields driven antiferromagnetic domain wall motions

W. H. Li, Z. Y. Chen, D. L. Wen, D. Y. Chen, Z. Fan, M. Zeng, X. B. Lu, X. S. Gao,
and M. H. Qin*

*Institute for Advanced Materials, South China Academy of Advanced Optoelectronics and
Guangdong Provincial Key Laboratory of Quantum Engineering and Quantum Materials,
South China Normal University, Guangzhou 510006, China*

[Abstract] In this work, we study the rotating magnetic fields driven domain wall motions in antiferromagnetic nanowires, using the numerical simulations of the classical Heisenberg spin model. We show that in low frequency region, the rotating field alone could efficiently drive the DW motion even in the absence of Dzyaloshinskii-Moriya interaction. In this case, the DW rotates synchronously with the magnetic field, and a stable precession torque is available and drives the DW motion with a steady velocity. In large frequency region, the DW only oscillates around its equilibrium position and cannot propagate. The dependences of the velocity and critical frequency differentiating the two motion modes on several parameters are investigated in details, which definitely provides useful information for future antiferromagnetic spintronics applications.

Keywords: antiferromagnetic domain wall, dynamics, rotating field

PACS numbers: 75.60.ch, 75.50.Ee, 02.60.-x

*Authors to whom correspondence should be addressed. Electronic mail: qinmh@scnu.edu.cn

I Introduction

Antiferromagnetic (AFM) materials are attracting more and more attentions due to their potential applications in the newly emerged AFM spintronics field.¹⁻³ Specifically, zero net magnetization and ultralow susceptibility in AFM elements of future storage devices allow significant improvement of performance stability against perturbing magnetic fields, as well as enhancement of element density without any stray fields.^{1,4} More importantly, faster magnetic dynamics than in ferromagnets makes AFM spintronics more promising.⁵ So far, several methods of modulating AFM domains and/or driving domain wall (DW) motion have been experimentally revealed or theoretically predicted.⁶⁻⁸

In experiments, it has been reported that the local staggered effective field in CuMnAs is induced by the applied electrical current through the spin-orbit effect, which modulates the orientation of the AFM moments.⁹ Similar behavior has been reported in Mn₂Au whose magnetic atoms are also with the locally broken inversion symmetry.¹⁰ More recently, the reversal of the magnetic domains in biaxial antiferromagnets NiO was realized by the current induced anti-damping torque.¹¹ Theoretically, the staggered field driven DW motion was investigated, and a high speed ~30 km/s was predicted partially attributing to the absence of walker breakdown which normally limits the velocity of typical ferromagnetic DW.⁷ Moreover, several external stimuli including spin wave excitations, field gradients, spin-orbit torques, and thermal gradients have been suggested to efficiently drive AFM DW motion.¹²⁻¹⁸ For example, AFM DW motion under an applied temperature gradient has been revealed to be determined by the competition between the entropic torque and the Brownian force.¹⁴

On the other hand, the Dzyaloshinskii-Moriya interaction (DMI) may lead to faster and more controllable motion of AFM DW. For instance, the DMI induces the spin rotation symmetry breaking, resulting in the strongly dependence of the DW motion on the polarization direction of the injected spin waves.^{17,18} Furthermore, the rotating magnetic field driven chiral DW motion has been also predicted in antiferromagnets with DMI, providing broad opportunities of controlling DW.¹⁹ It is suggested that the DMI plays an essential role in the motion, while the AFM DW in antiferromagnets without DMI may not be efficiently driven by the rotating field alone. Specifically, in order to explain this phenomenon, the AFM DW is regarded as a combination of a head-to-head DW and a tail-to-tail DW (move in opposite directions under rotating fields for the ferromagnetic case) on which the driven torques are well cancelled.

However, the AFM dynamics could be much more complex due to the strong coupling between two opposite magnetic sublattices, and the above explanation may not perfectly work. When a rotating field $\mathbf{h}(t)$ is applied, the precession torque $\sim -\mathbf{S} \times \mathbf{H}$ and the damping torque $\sim -\mathbf{S} \times (\mathbf{S} \times \mathbf{H})$ depending on spin \mathbf{S} and local effective field \mathbf{H} are induced on the central plane of the AFM DW (detailed definition will be given in the next section), as depicted in Fig. 1 which shows a Néel AFM DW in an AFM nanowire without DMI. It is well known that for an AFM system, applied field \mathbf{h} tends to align the spins in perpendicular to \mathbf{h} to save the Zeeman energy,²⁰ and the DW is expected to rotate synchronously with the rotating \mathbf{h} . As a result, a stable precession torque is available, resulting in an efficient DW motion. As a matter of fact, comparing with strong AFM exchange coupling, DMI may be too weak to be considered in a considerable number of antiferromagnets. Thus, there is still an urgent need to investigate the rotating field driven AFM DW motion in the absence of DMI.

In this work, we study the AFM DW motion driven by the rotating field using the Landau-Lifshitz-Gilbert (LLG) simulations of the classical Heisenberg spin model. We figure out that even in the absence of DMI, the rotating field in a low frequency could efficiently drive the DW motion with a steady velocity, while in large frequency region, the DW only oscillates around its equilibrium position and cannot propagate. The dependences of the velocity and the critical frequency on several parameters are investigated and discussed in detail.

II Model and method

We start from an AFM spin model with isotropic Heisenberg exchanges between the nearest neighbors and a uniaxial anisotropy term

$$H = J \sum_{\langle i,j \rangle} \mathbf{S}_i \cdot \mathbf{S}_j - d_z \sum_i (S_i^z)^2 - \sum_i \mathbf{h}(t) \cdot \mathbf{S}_i, \quad (1)$$

where $J > 0$ is the AFM coupling constant, $d_z > 0$ is the anisotropy constant defining an easy axis in the z (nanowire axis) direction, $\mathbf{S}_i = \boldsymbol{\mu}_i / \mu_s$ represents the normalized magnetic moment at site i with the three components S_i^x , S_i^y and S_i^z , $\mathbf{h}(t)$ is the circularly polarized magnetic field $\mathbf{h}(t) = h_0(\cos\omega t \cdot \mathbf{e}_x + \sin\omega t \cdot \mathbf{e}_y)$ with frequency ω and amplitude h_0 applied in the xy plane, as shown in Fig. 1.

The spin dynamics is investigated by the stochastic LLG equation,²¹⁻²³

$$\frac{\partial \mathbf{S}_i}{\partial t} = -\frac{\gamma}{\mu_s(1+\alpha^2)} \mathbf{S}_i \times [\mathbf{H}_i + \alpha(\mathbf{S}_i \times \mathbf{H}_i)], \quad (2)$$

where γ is the gyromagnetic ratio, α is the Gilbert damping constant, and $\mathbf{H}_i = -\partial H/\partial \mathbf{S}_i$ is the effective field. Unless stated elsewhere, the LLG simulations are performed on an one-dimensional lattice (lattice parameter a) with $1 \times 1 \times 1001$ spins with open boundary conditions using fourth-order Runge-Kutta method with a time step $\Delta t = 2.0 \times 10^{-4} \mu_s/\gamma J$, $d_z = 0.01J$, $\alpha = 0.01$, and $\gamma = 1$. After sufficient relaxation of the Néel AFM DW, $\mathbf{h}(t)$ is applied and the DW motion is studied.

III Simulation results and discussion

Fig. 2 presents the DW positions as a function of time for various ω for $h_0 = 0.1J$, which reveals two driven motion modes divided by a critical frequency ω_c . For a small ω below ω_c , $\omega = 0.05\gamma J/\mu_s$, for example, a rigid DW propagation with a constant drift velocity is observed, demonstrating that a rotating field alone can drive the AFM DW motion even in the absence of DMI. Similar to the chiral DW motion, the drift velocity increases with the increase of ω , as shown in Fig. 2(a). When ω is increased above $\omega_c \sim 0.098\gamma J/\mu_s$, the rotating field could not efficiently drive the DW anymore, and the DW only oscillates around its equilibrium position ($z = 505a$), as shown in Fig. 2(b) where gives the t -dependent DW positions for $\omega = 0.1\gamma J/\mu_s$. The velocity v as a function of ω for $h_0 = 0.1J$ is summarized in Fig. 2(c).

The simulated results can be qualitatively understood from the competing torques acting on the DW.¹³ When $\mathbf{h} = h_0(0, 1, 0)$ is applied, for instance, the precession torque \mathbf{T}_h^p and the damping torque \mathbf{T}_h^d are induced, as depicted in Fig. 2(d). Subsequently, the spins are driven slightly out of the easy plane, resulting in the additional precession torque \mathbf{T}_{ex}^p due to the strong AFM exchange interactions. It is noted that \mathbf{T}_{ex}^p is opposite to \mathbf{T}_h^p and quickly suppresses the total precession torque $\sim -\mathbf{S} \times \mathbf{H}$. As a result, a static field alone could not drive the DW motion, as has been explained in detail in our earlier work.²⁵ However, the effects of the rotating field on AFM dynamics are rather different. On the one hand, the rotating field \mathbf{h} tend to align the DW spins in perpendicular to \mathbf{h} to save Zeeman energy. However, the spin rotation is slightly behind \mathbf{h} (schematically depicted by $\Delta\delta = \delta - \delta'$ in Fig. 2(d)), leading to the fact that \mathbf{T}_h^p always defeat \mathbf{T}_{ex}^p and in turn resulting in a stable DW motion. Simultaneously, \mathbf{T}_h^d on the up spin is larger than that on the down spin. Thus, a net damping torque on the DW is generated and drive the DW synchronously rotates with \mathbf{h} . This argument has been confirmed by tracing the DW

profile and tilt angle ϕ which are respectively given in Figs. 3(a) and 3(b). The normalized staggered magnetization $\mathbf{n} = (\mathbf{S}_{2i} - \mathbf{S}_{2i-1}) / |\mathbf{S}_{2i} - \mathbf{S}_{2i-1}|$ for $\omega = 0.06\gamma J/\mu_s$ in Fig. 3(a) shows that n_x and n_y of the spins in the DW changes with time, demonstrating the rotation of the DW. The DW tilt angle linearly increases with t , as shown in Fig. 3(b), clearly demonstrating the perfect synchronized motion with the rotating field with a fixed phase difference ($\omega t - \phi$ approximately equals to δ). On the other hand, as ω increases, $\Delta\delta$ and the net precession torque $\mathbf{\Gamma}_h^p - \mathbf{\Gamma}_{ex}^p$ is increased, resulting in the enhancement of the DW motion along the nanowire. However, when ω is increased above the critical value, the DW spins cannot catch up with \mathbf{h} anymore ($\omega t - \phi$ changes with time for $\omega = 0.11\gamma J/\mu_s$ in Fig. 3(b)), and a periodic oscillating $\mathbf{\Gamma}_h^p$ is induced. Thus, the DW only oscillates around its equilibrium position and cannot propagate.

Subsequently, we investigate the dependences of the drift velocity v and the critical frequency ω_c on various parameters. Fig. 4(a) gives v as a function of ω for various h_0 , which clearly shows that both v and ω_c increases with the increasing h_0 . It is noted that the net precession torque is enhanced with h_0 , resulting in the increase of v for a fixed ω . Furthermore, the net damping torque on the DW is also increased, which in turn significantly enhances the rotation capability of the DW, resulting in the increase of ω_c . Moreover, the mobility of the AFM DW is significantly dependent on the energy of the DW E_{DW} , i. e., higher E_{DW} leads to lower mobility. This property is confirmed in our simulations, as shown in Fig. 4(b) where gives the $v(\omega)$ curves for various lattice sizes. It is noted that E_{DW} is extensively increased with the increase of the lattice size and dimension, resulting in the decrease of v for a fixed ω . Moreover, the rotation capability is also suppressed due to the enhancement of the exchange field, and ω_c decreases with the increasing lattice size.

Fig. 4(c) presents the simulated $v(\omega)$ curves for various d_z . Based on the continuum model, the DW energy can be estimated by $E_{DW} = 2\sqrt{2|J|d_z}$.²⁶ With the increase of d_z , the DW energy is increased, leading to the decrease of v for a fixed ω . Furthermore, the damping torque resulted from the exchange interaction $\mathbf{\Gamma}_{ex}^d$ is slightly suppressed and the net damping torque is strengthened, resulting in the enhancement of the DW rotation capability. In other words, the enhanced d_z could speed up the rotation of the spins around the z axis, allowing the DW catch up with \mathbf{h} easily and resulting in the increase of ω_c . On the other hand, the effects of the intermediate anisotropy constant d_x on the AFM dynamics of biaxial antiferromagnets are also investigated, and the corresponding results are given in Fig. 4(d). It is noted that an additional anisotropic energy $d_x \sum_i (S_i^x)^2$ barrier should be conquered during the rotation of the DW when a

nonzero d_x is considered, resulting in the suppression of the rotation capability. Specifically, the introduced d_x breaks the rotation symmetry of the DW, seriously impeding the synchronous rotation of the DW with \mathbf{h} . Thus, ω_c is significantly decreased with the increase of d_x . In addition, Γ_{ex}^p is slightly enhanced, and v slowly decreases as d_x increases.

In addition, it is noted that the damping term always impedes the spin precession and suppresses the DW mobility and rotation capability, resulting in the decreases of v and ω_c , the same as the earlier report.^{25,27} This behavior has been checked in our simulations, although the corresponding results are not shown here for brevity. Furthermore, we also investigated the dependence of the rotating plane of \mathbf{h} on the DW motion to figure out the optimal field orientation. The simulated results are presented in Fig. 5(a) where shows the $v(\omega)$ curves for various Φ (the angle between the rotating plane and xy plane). It is clearly shown that when the rotating plane deviates from the xy plane which is perpendicular to the spins in AFM domains, the DW motion is gradually suppressed. Moreover, the z -component of \mathbf{h} strongly destroys the AFM DW which could not be stabilized for a large ω .

So far, the rotating field driven AFM DW in the absence of DMI has been clearly demonstrated in our LLG simulations. Now, we can check the dependence of the DW dynamics on DMI which may be available in some realistic systems. Here, the DMI energy $\sum_i \mathbf{D}_i \cdot (\mathbf{S}_i \times \mathbf{S}_{i+1})$ with $\mathbf{D}_i = D(0, 0, 1)$ is considered, and the simulated results are presented in Fig. 5(b), where the $v(\omega)$ curves upon various D are plotted. The DW energy decreases to $E_{DW} = 2\sqrt{2|J|d_z - D^2}$,^{17,18,26} resulting in the increase of v for a fixed ω . Furthermore, a considerable v is obtained even for ω larger than ω_c in the presence of DMI. It is noted that the DMI induces the spin rotation symmetry breaking and stabilizes a chiral DW. Thus, even in the high frequency ($\omega > \omega_c$) region, a rather large net precession torque in one \mathbf{h} rotating period is available and drives the ratchet motion of the chiral DW.

IV Conclusion

In summary, we have studied the rotating field driven AFM DW motion using the LLG simulations of the classical Heisenberg spin model. It is revealed that even in the absence of DMI, the rotating field in the low frequency below ω_c could efficiently drive the DW motion. In this case, the DW rotates synchronously with the rotational field, and a stable precession torque is available and drives the DW motion with a steady velocity. In the large frequency

region, the DW only oscillates around its equilibrium position and cannot propagate. The dependences of the velocity and critical frequency on several parameters have been investigated in detail and qualitatively explained, which may provide useful information for future storage device design.

Acknowledgment

We are grateful for insightful discussions with Huaiyang Yuan, and Zhengren Yan. The work is supported by the National Key Projects for Basic Research of China (Grant No. 2015CB921202), and the Natural Science Foundation of China (No. 11204091), and the Science and Technology Planning Project of Guangdong Province (Grant No. 2015B090927006), and the Natural Science Foundation of Guangdong Province (Grant No. 2016A030308019).

References:

1. T. Jungwirth, X. Marti, P. Wadley, and J. Wunderlich, *Nat. Nanotechnol.* 11, 231 (2016).
2. A. H. Macdonald and M. Tsoi, *Phil. Trans. R. Soc. A* 369, 3098 (2011).
3. M. Stamenova, R. Mohebbi, J. Seyed-Yazdi, I. Rungger, and S. Sanvito, *Phys. Rev. B* 95, 060403(R) (2017).
4. J. Železný, H. Gao, K. Výborný, J. Zemen, J. Mašek, Aurélien Manchon, J. Wunderlich, Jairo Sinova, and T. Jungwirth, *Phys. Rev. Lett.* 113, 157201 (2014).
5. R. Cheng, D. Xiao, and A. Brataas, *Phys. Rev. Lett.* 116, 207603 (2016).
6. N. P. Duong, T. Satoh, and M. Fiebig, *Phys. Rev. Lett.* 93, 117402 (2004).
7. O. Gomonay, T. Jungwirth, and J. Sinova, *Phys. Rev. Lett.* 117, 017202 (2016).
8. B. G. Park *et al.*, *Nat. Mater.* 10, 347 (2011).
9. P. Wadley *et al.*, *Science* 351, 587 (2016).
10. T. Shiino, S. Oh, P. M. Haney, S. W. Lee, G. Go, B. G. Park, and K. J. Lee, *Phys. Rev. Lett.* 117, 087203 (2016).
11. X. Z. Chen, R. Zarzuela, J. Zhang, C. Song, X. F. Zhou, G. Y. Shi, F. Li, H. A. Zhou, W. J. Jiang, F. Pan, and Y. Tserkovnyak, *Phys. Rev. Lett.* 120, 207204 (2018).
12. S. K. Kim, O. Tchernyshyov, and Y. Tserkovnyak, *Phys. Rev. B* 92, 020402(R) (2015).
13. S. Selzer, U. Atxitia, U. Ritzmann, D. Hinzke, and U. Nowak, *Phys. Rev. Lett.* 117, 107201 (2016).
14. Z. R. Yan, Z. Y. Chen, M. H. Qin, X. B. Lu, X. S. Gao, and J. M. Liu, *Phys. Rev. B* 97, 054308 (2018).
15. E. G. Tveten, T. Muller, J. Linder, and A. Brataas, *Phys. Rev. B* 93, 104408 (2018).
16. E. G. Tveten, A. Qaiumzadeh, and A. Brataas, *Phys. Rev. Lett.* 112, 147204 (2014).
17. W. Yu, J. Lan, and J. Xiao, *Phys. Rev. B* 98, 144422 (2018).
18. A. Qaiumzadeh, L. A. Kristiansen, and A. Brataas, *Phys. Rev. B* 97, 020402 (2018).
19. K. Pan, L. Xing, H. Y. Yuan, and W. W. Wang, *Phys. Rev. B* 97, 184418 (2018).
20. O. Gomonay, M. Kläui, and J. Sinova, *Appl. Phys. Lett.* 109, 142404 (2016).
21. N. Kazantseva, U. Nowak, R. W. Chantrell, J. Hohlfeld, and A. Rebei, *Europhys. Lett.* 81, 27004 (2007).
22. D. Landau and E. Lifshitz, *Phys. Z. Sowjetunion* 8, 153 (1935).
23. T. L. Gilbert, *IEEE Trans. Magn.* 40, 3443 (2004).
24. W. F. Brown, *Phys. Rev.* 130, 1677 (1963).

25. Z. Y. Chen, Z. R. Yan, Y. L. Zhang, M. H. Qin, Z. Fan, X. B. Lu, X. S. Gao and J.-M. Liu, *New J. Phys.* 20, 063003 (2018).
26. C. Mitsumata and A. Sakuma, *IEEE Trans. Magn.* 47, 3501 (2011).
27. S. Moretti, M. Voto, and E. Martinez, *Phys. Rev. B* 96, 054433 (2017).

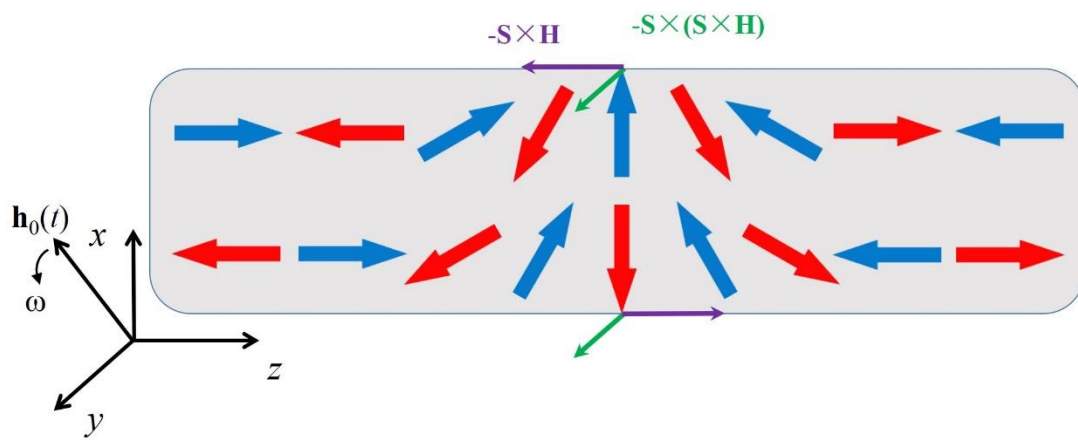


Fig.1. (color online) Sketch of the torques acting on the central plane of a domain wall under a rotating magnetic field. The two sublattices of the AFM are occupied with blue and red spins, respectively. The rotating field in the xy plane is also depicted.

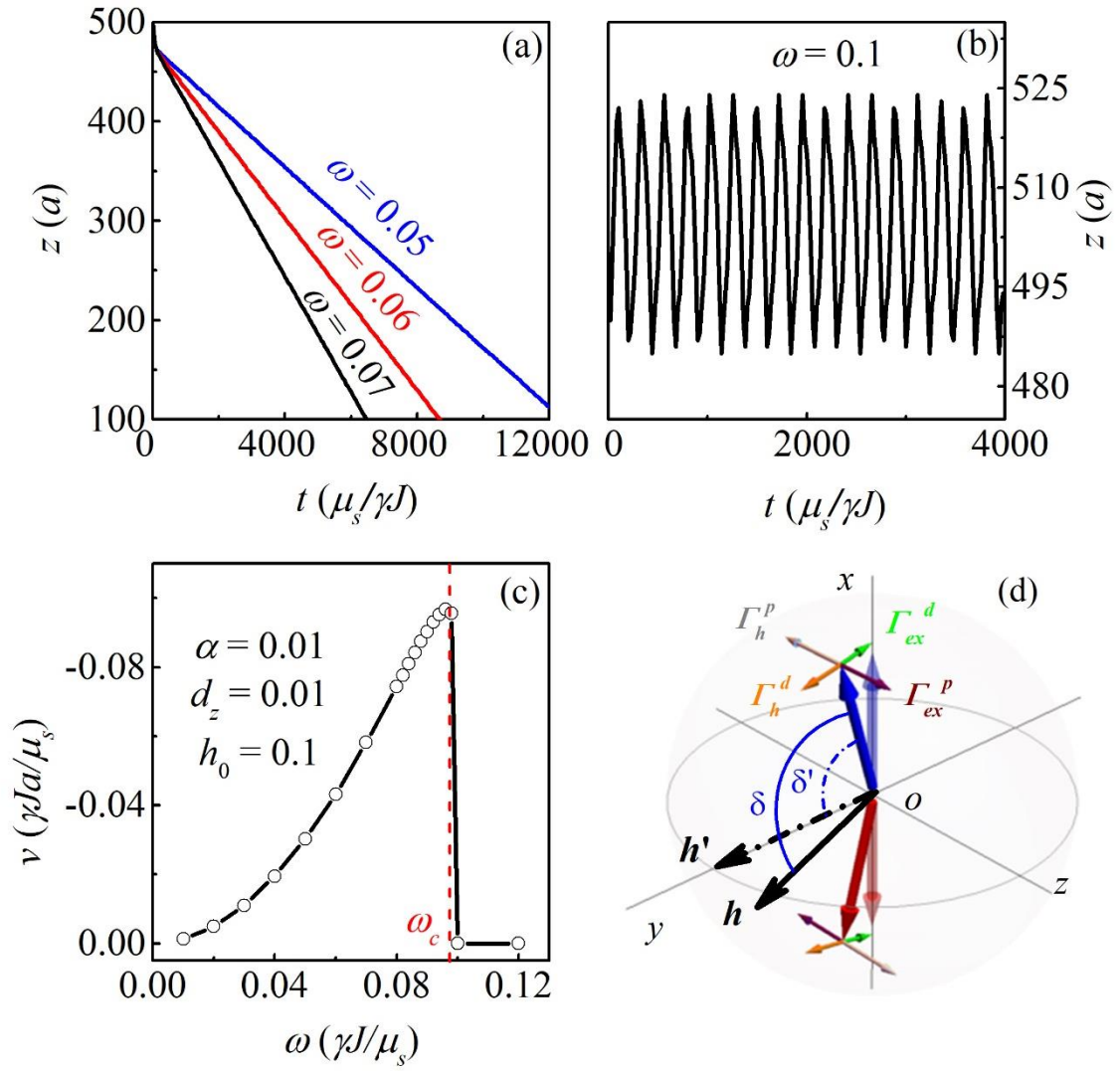


Fig.2. (color online) The domain wall position as a function of time t for (a) $\omega = 0.05, 0.06$ and 0.07 , and (b) $\omega = 0.1$ at $h_0 = 0.10$. (c) The calculated DW drift velocity v as a function of ω under $h_0 = 0.1$, and (d) a schematic depiction of the torques acting on the central plane of a DW under a rotating field.

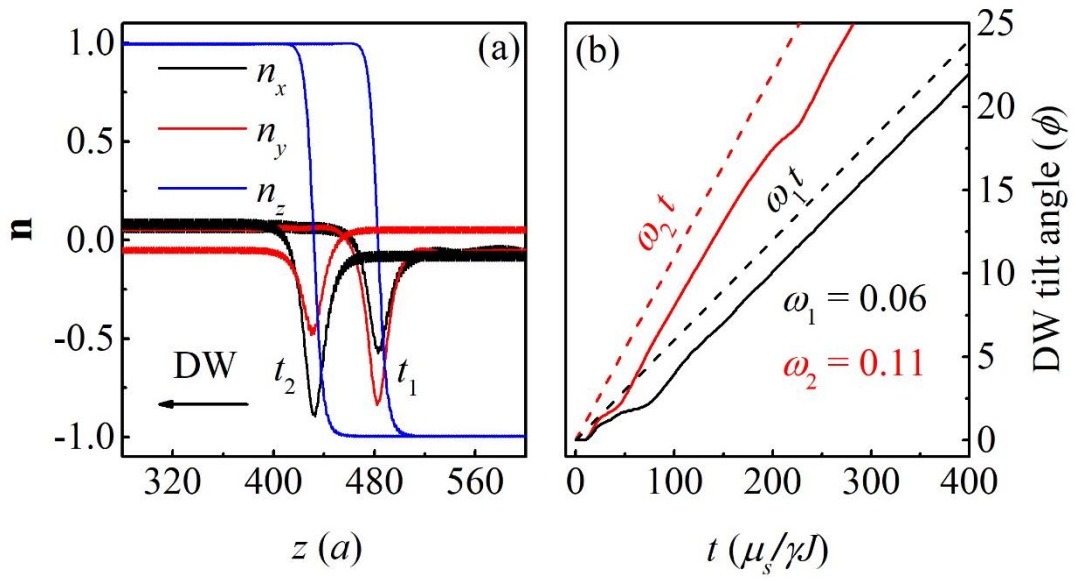


Fig.3. (color online) (a) The domain wall profiles for $\omega = 0.06$ at t_1 and t_2 , and (b) the DW tilt angle as a function of time for $\omega_1 = 0.06$ and $\omega_2 = 0.11$. The phases $\omega_1 t$ and $\omega_2 t$ are also given for an easy comparison.

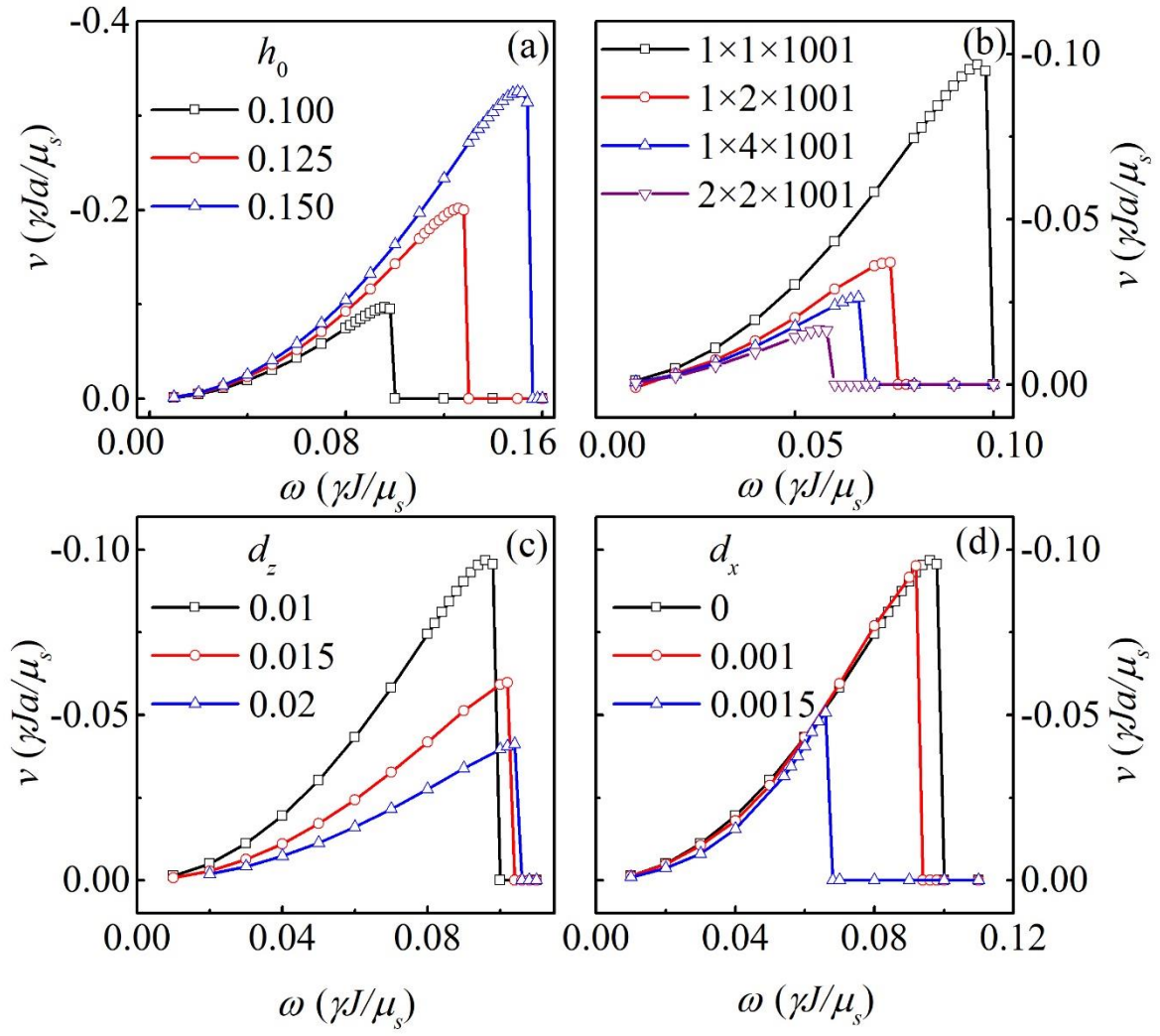


Fig.4. (color online) The calculated $v(\omega)$ curves (a) for various h_0 , and (b) for various lattice sizes, and (c) for various d_z , and (d) for various d_x for $d_z = 0.01$.

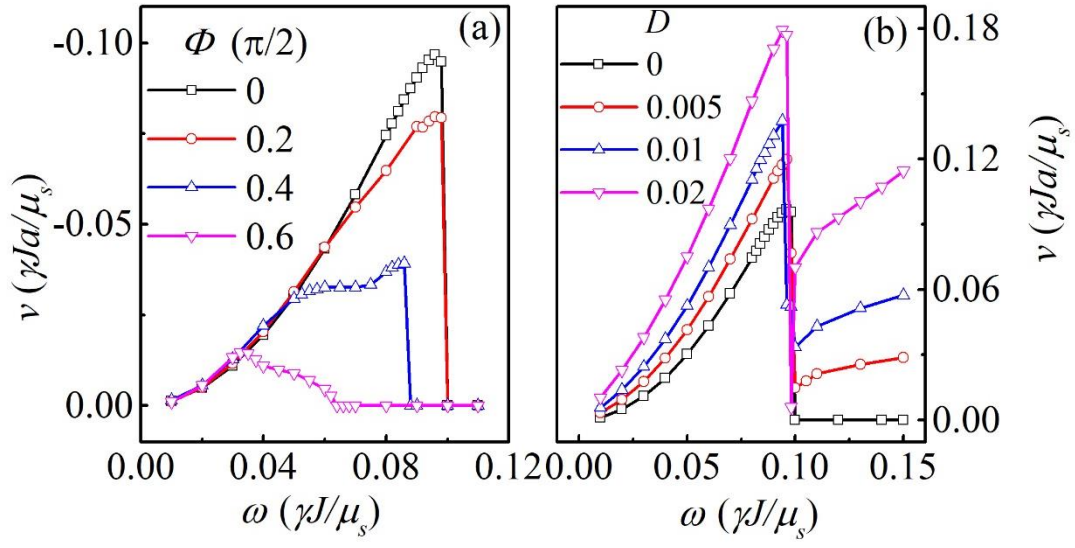


Fig.5. (color online) The calculated $v(\omega)$ curves (a) for various Φ , and (b) for various DMI constants D .